A novel self-organizing embryonic stem cell system reveals the role of Wnt signaling parameters in anterior-posterior patterning of the nervous system

Siqi Du[1] and Aryeh Warmflash[1]

Abstract

A Wnt activity gradient is essential for the formation of the anterior-posterior (AP) axis in all vertebrates. The relationship between the dynamics of Wnt signaling and specification of AP coordinates is difficult to study in mammalian embryos due to the inaccessibility of developing embryos and the difficulty of live imaging. Here, we developed an *in vitro* model of human neuroectoderm patterning, where the AP axis self-organizes along the radius of a micropatterned human pluripotent stem cell colony. We used this system to study the quantitative relationship between Wnt signaling in space and time and the resulting AP patterns. We found that rather than a smoothly varying gradient along the axis, signaling is elevated in midbrain compared to either surrounding region. The timing, rather than the amplitude or duration, of the Wnt response played the most important role in setting axial coordinates. These results establish a simple system for studying the patterning of the human nervous system and elucidate how cells interpret Wnt dynamics to determine their position along the AP axis.

Keywords: AP axis formation, Neuroectoderm development, Wnt signaling, Midbrain-hindbrain border

1 Introduction

Establishing the anterior-posterior (AP) axis is a fundamental step in defining the body plan of all vertebrates (Yamaguchi, 2001). The central nervous system originates from the ectodermal germ layer and is compartmentalized along this axis into the forebrain, midbrain, hindbrain, and spinal cord. To establish the AP pattern within the neuroectoderm, pluripotent cells from the epiblast must both be converted to neural fates and assigned axial coordinates. The experiments of Spemann and Mangold demonstrated the existence of an organizer in amphibians capable of converting cells to neural fates within the ectoderm (Hamburger, 1989; Spemann and Mangold, 1924). This neuralizing ability results from secreted inhibitors, and inhibition of both branches of the TGFβ pathway—Activin/Nodal and BMP—is sufficient to convert cells to anterior neural fates in multiple vertebrate models, including human pluripotent stem cells (hPSCs) (Camus et al., 2006; Chambers et al., 2009; Fainsod et al., 1997; Di-Gregorio et al., 2007; Hammerschmidt et al., 1996; Sasai et al., 1994; Schulte-Merker et al., 1997; Smith and Harland, 1992). This suggests that the anterior fate is the default, and posteriorizing signals are required to establish the axis, consistent with the activation-transformation model originally proposed by Nieuwkoop (Nieuwkoop, 1952; Nieuwkoop and Nigtevecht, 1954). More recently, lineage tracing experiments as well as measurements of chromatin accessibility have suggested that cells in the posterior region acquire regional identity before neural identity and cells of spinal cord share a common lineage with the somitic mesoderm rather than with more anterior neural fates (Gouti, Tsakiridis, et al., 2014; Metzis et al., 2018; Tzouanacou et al., 2009).

The molecular identity of the caudalizing signal has long been a central question in developmental biology. Many candidates have been proposed, including Wnts, FGFs, and retinoic acid (RA) (Stern, 2001). Among them, the Wnt pathway has the ability to affect the entire AP axis without interfering with neural induction (Kiecker and Niehrs, 2001; Kumar et al., 2021; P. Liu et al., 1999; Maden, 2002). Multiple Wnt ligands are expressed in the posterior region of the embryo (Andre et al., 2015; Christian et al., 1991; Hong et al., 2008; Kelly et al., 1995; Krauss et al., 1992; Moon et al., 1993). Meanwhile, Wnt antagonists are found in the anterior region and are critical for head induction (Bouwmeester et al., 1996; Glinka et al., 1998; Leyns et al., 1997; Shibata et al., 2005; Wang et al., 1997; Yamamoto et al., 2005).

[1]Rice University (Siqi.Du@rice.edu; aryeh.warmflash@rice.edu)

Beyond the expression patterns of Wnts and their inhibitors along the AP axis, functionally, an endogenous activity gradient of Wnt/β-catenin aligns with AP axis, and is indispensable for proper patterning (Glinka et al., 1998; Kiecker and Niehrs, 2001; Kimura-Yoshida et al., 2005).

Stem cell models are powerful tools for studying mammalian embryos, which are otherwise difficult to access *in vivo* (Fu et al., 2021; Rossant and Tam, 2021). PSCs have great potential to differentiate into a variety of cell fates, including ordered arrangements of multiple cell fates. hPSCs treated with dual-Smad inhibition are efficiently converted to neural fates (Chambers et al., 2009). Such protocols have been combined with microfluidics to create bioengineered models of the developing neural tube that successfully recapitulate the cell fates along the AP axis (Rifes et al., 2020; Xue et al., 2024). In these models, the gradients used to establish the axes are externally imposed and so they do not mimic the self-organization of gradients which occurs *in vivo*. We sought to create a self-organizing *in vitro* model system to study patterning along the AP axis with minimal external spatial cues.

Our previous work and that of others showed that globally applying pathway activators or inhibitors to geometrically confined hPSC cultures can recapitulate germ layer patterning as well as mediolateral patterning within the ectoderm depending on the protocol (Fig. 1A, Britton et al., 2019; Haremaki et al., 2019; Jo et al., 2022; Karzbrun et al., 2021; Martyn et al., 2019; Minn et al., 2020; Warmflash et al., 2014). These micropatterned systems generate dynamic signaling patterns starting from the edge (Chhabra et al., 2019; Heemskerk et al., 2019), and we reasoned that self-organized Wnt activity patterns within the neuroectoderm could be generated in a similar manner. In this study, we show that treating colonies differentiating to neural fates with Wnt ligands creates self-organized patterns of cell fates corresponding to the AP axis within the neuroectoderm. Comparison with single-cell RNA sequencing data from mouse embryos (Pijuan-Sala et al., 2019), revealed that this system successfully replicates the spatial and temporal emergence of cell fates along the AP axis. We used this system to quantitatively dissect the relationship between Wnt signaling dynamics and cell fates and found that the timing of Wnt signaling, rather than the magnitude or duration, defines the boundary between the midbrain and hindbrain. Our system also revealed that rather than monotonically increasing Wnt activity from anterior to posterior, the midbrain region has higher Wnt activity than either of the neighboring territories. These findings highlight the power of self-organizing systems to dissect both the development and interpretation of signaling patterns along the AP axis.

2 Results

A micropatterned model of AP patterning within the nervous system

We sought to create a model in which as much of the AP axis ranging from forebrain to spinal cord is recapitulated along the radius of an hPSC colony. Based on earlier work with micropatterns, we anticipated that added Wnt ligands would signal most strongly at the colony edge, conferring posterior identities there while allowing more anterior fates to develop at the center. Therefore, we performed a neural induction protocol on micropatterns and treated the colonies with WNT3A to induce an underlying gradient of Wnt activity and promote AP axis patterning (Fig. 1B, Fig. S1A). We use OTX2 to mark anterior cell fates, and HOXB1 and HOXB4 to mark posterior cell fates. Under WNT3A treatment, the colony forms concentric rings of HOXB1 and HOXB4, with HOXB1 extending further toward the colony center. This validates that adding Wnt posteriorizes the colony edge more strongly than the center, generating cell fates that are spatially organized along the AP axis. The absence of OTX2, however, indicates that this protocol fails to generate the most anterior cell fates, including forebrain and midbrain. We hypothesized that delaying the addition of Wnt might allow some cells to commit to anterior fates, preventing the posteriorization of the entire colony in response to Wnt. To test this, we added WNT3A after 1, 1.5, or 2 days of neural differentiation and examined cell fates after 4 days (Fig. 1C). When Wnt was added after 1 day, small, irregular patches of cells expressed OTX2 near the colony center. When addition was delayed by 1.5, a circular domain of cells expressed OTX2 in the center with rings of HOXB1 and HOXB4 expression near the edge. If addition was further delayed to 2 days, the domain of OTX2 expanded further but HOXB4 disappeared. Thus, later Wnt addition produces progressively more anterior patterns. We found that addition of WNT3A at day (D) 1.5 is optimal for obtaining the broadest range of cells fates along the AP axis.

The model recapitulates the dynamics of gene expression that occur *in vivo*

Having demonstrated that the micropatterned system generates cell fates corresponding to a broad range of the AP axis, we next asked how accurately it reflects the dynamics of the emergence of a larger set of genes that mark more specific regions of the nervous system, compared to the mammalian embryo *in vivo*. We obtained a publicly available

single-cell (sc) RNA sequencing dataset of mouse embryos collected from embryonic day (E) 6.5 to E8.5, a time period which spans the transition of the epiblast into patterned neuroectoderm, matching the processes which occur in the micropatterned culture system (Pijuan-Sala et al., 2019). We selected the five relevant cell fate groups which represent the neuroectoderm and its precursors (rostral neuroectoderm, caudal neuroectoderm, forebrain/midbrain/hindbrain, spinal cord, and neuromesodermal progenitors (NMP)) and performed scVI normalization and UMAP visualization. This visualization resulted in a clear ordering of the cells in space along the first UMAP coordinate and in time along the second (Fig. 2A). In time, cells first express the pluripotency marker *Pou5f1* (*Oct4*) along with *Cdh1* (Ecad). The expression of these genes decreases as *Cdh2* (Ncad) expression increases, an early indicator of neural differentiation. This transition happens slightly earlier in the anterior than in the posterior (Fig. 2B). From anterior to posterior (right to left on the UMAP plot), the anterior marker *Otx2* is expressed, followed by *Pax5*, which emerges near the caudal midbrain/rostral hindbrain region, and then the posterior markers *Hoxb1*, *Hoxb4*, and *Cdx2* (Rowitch and McMahon, 1995, Fig. 2B). *Otx2* is expressed during gastrulation and later becomes restricted to the anterior region of the neuroectoderm. In the posterior of the embryo, *Cdx2* expression precedes that of the Hox genes, and *Hoxb1* precedes *Hoxb4*.

For comparison, we performed immunostaining of the same markers in our *in vitro* system at each day from D1 to D5 (Fig. 2C-C', Fig. S1B-B'). OCT4 is downregulated after D3, while NANOG is only expressed on D1. SOX2 is continuously expressed throughout the colony with expression levels that vary differently depending on the radial coordinate. The switch between ECAD and NCAD occurs on D3, although there remains a belt of lower NCAD expression midway through the colony. Among the markers representing AP identities, OTX2 emerges first on D2, followed by HOXB1 and CDX2 on D3, HOXB4 on D4, and PAX5 between D4 and D5. All of these trends are consistent with the *in vivo* mouse scRNA dataset and literature on the expression patterns of these specific genes (Kessel and Gruss, 1991; Pannese et al., 1995; Simeone, Acampora, Mallamaci, et al., 1993). Thus, the *in vitro* micropatterned system not only recapitulates the spatial ordering of markers from anterior to posterior, but also reproduces the dynamics of cell fate decisions. There is a rough correspondence between timing where D1 corresponds to E6.5, D2 to E6.75–E7.5, D3 to E7.5–E8.0, D4 to E8.0–E8.25, and D5 to E8.5.

The isthmic organizer is located near the midbrain-hindbrain border (MHB), which is denoted by a sharp boundary in Otx2 expression (Simeone, Acampora, Gulisano, et al., 1992). The midbrain marker *Wnt1* and the isthmic organizer marker *Fgf8* are expressed in adjacent stripes near the MHB (Broccoli et al., 1999; Canning et al., 2007, Fig. 2E). We performed fluorescent in situ hybridization for these genes and found this organization is well preserved in our system (Fig. 2F). Moreover, we found that when colonies were treated with IWP2 (a Wnt inhibitor) rather than Wnt activation during neural induction, *WNT1* expression was lost but *FGF8*-expressing cells filled the colony, consistent with the expression of this gene in the anterior forebrain (Shimamura and Rubenstein, 1997, Fig. 2G). Taken together, our results show that the micropatterned model creates patterns that faithfully recapitulate a wide range of fates along the AP axis and this range can be shifted either anteriorly or posteriorly by changing Wnt activity levels.

Quantitative relationship between Wnt signaling parameters and AP pattern

Having established that Wnt is a crucial parameter for controlling AP patterning in our system, as it is *in vivo*, we examined how the parameters of Wnt stimulation influenced the patterns that form by varying the concentration, duration, or timing of WNT3A presentation, and observing the resulting AP patterning (Fig. 3, Fig. S2). First, we added WNT3A on D1.5 as above, varying the concentration from 0 to 1000 $\mathrm{ng/mL}$. As the concentration increased, the OTX2 and PAX5 domains shrank and disappeared when Wnt levels exceeded 300 $\mathrm{ng/mL}$, while the HOXB1 and HOXB4 domains expanded from the edges, and their expression levels increased. This demonstrates that higher Wnt concentrations lead to more posterior regions of patterning in a graded fashion (Fig. 3A-A', Fig. S2A-A'). Second, we tested the timing of Wnt addition. The colony was treated with WNT3A for 24 hours, starting at D0, D1, D2, or D3 (Fig. 3B). The MHB, represented by the gap between OTX2 and HOXB1, shifted dramatically depending on the timing of Wnt addition, with later addition shifting this boundary outwards so that anterior fates filled a large fraction of the colony. Third, we examined the effect varying the duration of Wnt exposure. WNT3A was added on the same day but removed on different days, resulting in varying treatment durations. Surprisingly, the anterior marker OTX2 was solely affected by the timing of Wnt addition (Fig. 3D-D'). When Wnt was added on D0, no OTX2 was expressed, even if Wnt was only present for one day. When Wnt was added on D1, OTX2 remained in the center; when added on D2, OTX2 occupied a much larger territory. The data on the effects of timing and duration on OTX2 expression are summarized in Fig. 3D' where the curves group by the starting time, rather than the ending time or duration. The posterior cell fates which form at the edge of the colony become progressively more posterior with longer WNT3A

exposure, however, the position of the boundary between posterior and anterior fates remains the same. This effect is particularly evident in HOXB4 with treatment beginning on D0 where anterior fates do not form. With increasing duration, the peak in HOXB4 expression shifts inward reflecting a posterior shift in these cell fates (Fig. 3E-E'). Thus, among the three factors, timing is the strongest determinant of whether cells adopt anterior or posterior fates, while concentration and duration have graded effects with increasing concentration or duration leading to a shift to more posterior cell fates.

AP pattern partially scales with colony size

Previous work on gastrulation stage micropatterns has shown that the scale of the pattern remains the same as the size of the colony is varied (Warmflash et al., 2014). As a result, when the colony becomes sufficiently small, the cell fates at the center are lost. An alternative is known as scaling in which the scale of the cell fate pattern changes to match the available space within the tissue or colony. To investigate these issues in the context of AP patterning, we grew hPSCs on micropatterned colonies, ranging in size from 50 to 500 μm, and observed the markers of AP patterning (Fig. 4A-A'). In the largest colonies, the width of the HOXB1 ring is approximately 150 μm so that if the scale of patterning remained invariant, we would expect the HOXB1 expressing region to cover the colony and the OTX2 expressing region to be lost in colonies with radii less than this size. However, colonies of radius 100 μm still display a ring-shaped HOXB1 domain suggesting that this territory becomes smaller, scaling with the smaller size of the colony. Nonetheless, OTX2 is completely lost in colonies of radius 50 or 100 μm indicates that this scaling is only partial rather than always restoring the complete patterning. At 250 μm, the OTX2 peak shifts slightly outward compensating for some of the loss of territory in the colony, which is also consistent with partial scaling.

To better understand these observations, we examined Wnt signaling activity along the colony radius by measuring the expression of LEF1, a direct Wnt target, and simultaneously measuring the dynamics of AP coordinate acquisition (Fig. 4B-B'). A gradient forms by D2 with changes in shape on D3–D4. Colonies with smaller radii require more time to stabilize their gradient (Fig. 4B') initially showing more homogeneous signaling before it is reduced at the colony center. HOXB1 emerges on D3 with a similar spatial pattern to LEF1. This relationship remains consistent on D4, except that LEF1 levels are slightly elevated in the center of the colony, forming a valley-like region of Wnt activity (discussed in the next section). There is no corresponding elevation in HOXB1 expression as the center of the colony retains an anterior coordinate. When comparing colonies of different radii, smaller ones exhibit higher LEF1 levels and steeper LEF1 gradients (Fig. S3A). Also, higher LEF1 levels overall lead to increased HOXB1 expression (Fig. 4B-B'). On D4, even the lowest LEF1 level in r50 is higher than the peak value observed in other conditions; however, the lower LEF1 expression at the colony center does correlate with reduced HOXB1. This provides strong evidence that cell fate decisions are not solely based on strict thresholding of Wnt activity, but rather on discerning the differential levels within the cell and its surroundings, allowing the overall pattern to partially scale with colony size.

Wnt activity gradient does not increase monotonically along the AP axis

The Wnt activity gradient which rises from anterior to posterior is present in nearly all bilaterally symmetric animals (Petersen and Reddien, 2009). While it is generally assumed that Wnt activity varies smoothly along the axis, we found in Fig. 4B' that LEF1 expression dips on D4 near the MHB in colonies of sufficient size to form both anterior and posterior cell fates. To see whether this reflects Wnt activity more generally, we measured the levels of *AXIN2*, another direct Wnt target, and found a similar trend, suggesting that Wnt activity does not vary monotonically along the axis but is elevated near the MHB compared to either of the surrounding regions (Fig. S3B-C, E). Within the central territory of the colony there are regions that lack both OTX2 and *WNT1* expression as well as forebrain markers PAX6 and FOXG1, suggesting that these regions are more posterior than the neighboring midbrain which expresses OTX2 (Fig. 4D, Fig. 2F, Fig. S1A). Interestingly, the OTX2-expressing area has a higher *AXIN2* level than the non-OTX2-expressing area (Fig. 4D, Fig. S3F) with a strong correlation between *AXIN2* and OTX2 expression within the colony center (Fig. 4E). Thus the OTX2 expressing midbrain territory shows higher Wnt signaling levels than the more posterior anterior hindbrain found in immediate juxtaposition. We examined whether these expression trends hold true within the mouse scRNA dataset and found that both *Lef1* and *Axin2* show elevated Wnt activity near the MHB compared to the surrounding regions (Fig. 4C, Fig. 2E), suggesting a potential relationship between elevated Wnt activity in the midbrain and MHB formation.

Wnt signaling at different times has similar dynamics but different outcomes

The level of Wnt signaling and cell fates at the end of patterning are not always correlated. For example, when cells were treated with Wnt on different days, treatment from D0 to D1 shows the strongest posteriorization but the lowest Wnt signaling activity (Fig. S4B-B'). This suggests the need to consider the signaling history of cells to understand the resulting patterns. To measure Wnt dynamics, we used H9 cells with GFP fused to histone H2B under the control of a TCF/LEF1-responsive promoter (Zheng et al., 2019), which gave similar patterns of AP fates compared to the experiments with ESI017 above (Fig. S4A-C', Fig. S2). We monitored Wnt signaling dynamics while exposing cells to WNT3A for 24 hours varying the timing of its addition during differentiation. WNT3A addition triggered an expanding front of Wnt activity which originates from the colony edge and travels inward, reaching approximately 100 μm into the colony. Cells respond rapidly upon Wnt addition and signaling continues throughout differentiation with peak levels of the reporter reached after about 24–48 hours and signaling declining somewhat thereafter (Fig. 5A). Although the amplitude of the response varies depending on the day of Wnt addition, the overall dynamics remain consistent (Fig. 5B). We then investigated the dynamics under varying durations of Wnt exposure. Longer exposure leads to a stronger and more prolonged response; nonetheless, the response peaks at approximately 24 hours and then declines. Notably, the signaling wave does not extend beyond 100 μm from the colony edge (Fig. 5C-D) when varying the timing or duration, but increasing the concentration of Wnt allows the signaling wave to reach further inward (Fig. S4D-E).

We examined the relationship between time of Wnt addition, the response amplitude, and the resulting patterns (Fig. 5E) across all live imaging experiments where duration and timing of Wnt were varied. The response was strongest when Wnt was added on D1 with weaker responses when added earlier or later, suggesting that there is a temporal window during neural differentiation when cells are more responsive to Wnt treatment. As the shape of the response curve remains consistent, the two major characteristics of the Wnt response are the amplitude and timing of the curve and we plotted them against the distance of the cell fate border from the edge (Fig. 5F). Later Wnt signaling causes an outward shift in the cell fate boundary which linearly depends on the timing. In contrast, there was no clear relationship between the peak amplitude and the boundary position. We conclude that the timing of the Wnt signaling determines the location of the MHB.

3 Discussion

We developed a system in which human pluripotent stem cells (hPSCs) differentiate to neural precursors, forming a self-organized anterior-posterior (AP) axis which aligns with the radial coordinate of a two-dimensional colony. From the center to the edge, cell fates became progressively more posterior. We used dual-Smad inhibition to induce neural conversion of hPSCs and subsequently treated the colonies with WNT3A to induce axial identities. By comparing with available scRNA expression data, we showed that this system successfully recapitulates spatial and temporal patterns of gene expression in the developing mammalian nervous system. We used this system to determine the quantitative relationship between Wnt ligand presentation, the dynamics of signaling activity, and AP patterning. The timing of Wnt introduction was a critical parameter, and delaying Wnt allowed central cells to commit to anterior fates while edge cells were posteriorized. The later the introduction of Wnt, the larger the region of anterior differentiation. The system's self-organizing nature distinguish it from recent models in which Wnt gradients are generated using microfluidic devices in order to impose an AP axis (Rifes et al., 2020; Xue et al., 2024). The self-organized patterns of Wnt activity are more complex than a simple gradient increasing from anterior to posterior and more closely mimic the *in vivo* situation (as shown in Fig. 2).

Multiple models have been proposed to explain how the pluripotent cells of the epiblast are both converted to neural fate and acquire their position along the AP axis. The classic model is that cells are first specified to anterior neural identity and then cells outside the forebrain are posteriorized according to their position along the axis (Nieuwkoop and Nigtevecht, 1954; Stern, 2001, 2006). Emerging evidence challenges this view, suggesting that hindbrain and spinal cord are specified as posterior before acquiring neural identity (Gouti, Tsakiridis, et al., 2014; Metzis et al., 2018; Tzouanacou et al., 2009). The expression of AP position markers such as OTX2 and HOXB1, overlapping in time with pluripotency-associated genes such as OCT4 and ECAD, and well before the emergence of neural fate markers such as SOX1 or PAX6, provide further support for the idea that acquisition of the AP coordinate precedes neural differentiation (Fig. 2B-C, Fig. S1).

The role of Wnt signaling in the establishment of the AP axis is remarkably conserved across the animal kingdom and involves the posterior expression of Wnt ligands and the anterior expression of Wnt inhibitors, which results in

the formation of a Wnt activity gradient (Kiecker and Niehrs, 2001; Petersen and Reddien, 2009). Measurements of signaling activity in our system, however, reveal that the Wnt profile does not simply increase along the axis. Instead, Wnt activity levels in the midbrain region are higher than the adjacent regions, creating a dip in the overall "gradient" which aligns with the anterior hindbrain. Examining scRNA expression data from the mouse embryo, we found that the expression of Wnt targets follows a similar pattern along the AP axis (Fig. 4B-E). There have been many hypotheses about how the midbrain-hindbrain border (MHB) is developed and maintained (Rhinn and Brand, 2001). Based on the stage this dip in Wnt activity appears, we propose that the MHB may align with a localized rise in Wnt signaling in the anterior direction which contrasts it from the remainder of the axis in which Wnt signaling declines in the anterior direction. In order to validate this idea, Wnt signaling needs to be manipulated in space to alter its profile along the axis. For example, elevating Wnt signaling in the anterior hindbrain to match the midbrain could test whether the MHB is still maintained without a spatial gradient in the opposite direction from the remainder of the axis.

In this study, we primarily focused on generating patterns that span from anterior (OTX2 expressing) to posterior (HOX gene expressing) fates but the system does not form the most anterior forebrain (FOXG1 expressing) or the most posterior parts of the spinal cord. However, we showed that the region spanned by the axis of the micropatterned colony is tunable. Tuning the timing, levels or durations of WNT3A treatment, can shift the system to different ranges of the AP axis. Furthermore, when WNT3A is replaced with IWP2 (a Wnt inhibitor), the colony is composed of the most anterior neural (telencephalic) cell fates (Fig. 2G). This broadens the application of our system for studying AP patterning. The failure to generate the more posterior spinal cord fates may be due to the need to both generate and maintain neuromesodermal progenitors (NMPs) to access more posterior regions of the spinal cord (Gouti, Delile, et al., 2017; Gouti, Tsakiridis, et al., 2014; Lippmann et al., 2015; Tsakiridis et al., 2014; Tzouanacou et al., 2009) as well the need for longer culture times to allow this posteriorization to occur. It is possible that with the addition of FGF signaling, our system could sustain NMPs at the colony edge allowing the cells to posteriorize further before neural differentiation. Our recent work on micropatterns, however, showed difficulty in maintaining NMPs and treatment with Wnt and FGF together resulted in either endoderm or paraxial mesoderm differentiation depending on the state of the Nodal pathway (Ortiz-Salazar et al., 2024).

Micropatterned colonies self-organize into patterns of cell fates in a variety of contexts including germ layer patterning, medial-lateral patterning of the ectoderm, and the anterior-posterior patterns described here (Fig. 4, Britton et al., 2019; Chen et al., 2025; Martyn et al., 2019; Warmflash et al., 2014). In all of these systems, exogenous signals are most strongly received at the edge of the colony which then serves as a signaling center, initiating cascades of endogenous signals and creating patterns (Chhabra et al., 2019). This organization may mimic tissue boundaries in the embryo, for example, the boundary between the amnion and epiblast during germ layer patterning. A disadvantage, however, is the inability to generate multiple signaling centers. This limitation may prevent the system from modeling the entire AP axis at once as it requires both Wnt activators and inhibitors to achieve the full complement of cell fates. Juxtaposing multiple cell populations expressing different molecules, as well as using optogenetic tools, are both promising approaches for exploring systems with multiple sources of signaling molecules (Emiliani et al., 2022; L. Liu et al., 2022). For example, using juxtaposition, one could place cells differentiating toward neural fates between two populations, one expressing Wnt activators and the other expressing Wnt inhibitors. Alternatively, using the AP patterning system developed here while optogenetically inducing Wnt inhibitors at the colony center may allow for a more complete recreation of the AP axis.

Although only capturing part of the AP axis at a time, our system has allowed us to dissect how parameters of Wnt signaling influence pattern generation. In the future, we can use this system and its variants to explore how Wnt interacts with other pathways such as FGF and retinoic acid to fully pattern this axis.

4 Materials and Methods

Cell lines

Experiments were performed using ESI017 hESCs (obtained from ESI BIO, RRID: CVCL_B854, XX) unless otherwise noted. For live imaging of WNT signaling dynamics, the H9 TCF/LEF:H2B-GFP reporter cell line was used (Zheng et al., 2019).

Routine cell culture

All cells were grown in the chemically defined medium mTeSR1 (STEMCELL Technologies) and kept at 37°C, 5% CO_2. Cell culture dishes were coated with Matrigel/Geltrex (Corning; 1:500 diluted in PBS-- and incubated at 4°C overnight). Cells were regularly checked for pluripotency and mycoplasma contamination throughout the study. Dispase (STEMCELL Technologies; 1:5 dilution in DMEM/F12 (VWR)) was used for gentle dissociation and routine passage. Accutase (Corning) was used to prepare single-cell suspensions. ROCK-inhibitor Y27672 (STEMCELL Technologies; 10 µm, diluted 1:1000) was used to reduce dissociation-induced apoptosis during single-cell suspension.

Micropatterning

Micropatterning experiments were performed on either micropatterned chips or 96-well micropatterned plates from CYTOO.

For chips, hESCs were seeded onto micropatterned surfaces coated with 5 µg/mL LN-521. The modified mTeSR1 protocol from Deglincerti et al., 2016 was used with the following modifications: 1) the chip was incubated for 3 h at 37°C during coating; 2) the chip was washed eight times with PBS++ (cytiva); 3) 1×10^6 cells were deposited onto the chip using a circular motion; 4) seeded cells were incubated for 1.5 h at 37°C, followed by two partial washes and one full wash (4 mL pre-warmed PBS-- in each wash).

For 96-well plates, hESCs were seeded onto micropatterned surfaces coated with 50 µL of 5 µg/mL LN-521 (Biolamina; diluted in PBS++) and incubated for 2.5 h at 37°C or overnight at 4°C. The LN-521 was removed by three partial washes and one full wash (100 µL PBS++ in each wash, except the first wash which was 150 µL). The plate was either used immediately or stored for up to 2 weeks at 4°C with PBS++ covering the surfaces. For seeding, cells were washed twice with PBS-- and removed from the surface using Accutase (Corning) for 5-7 min at 37°C. Subsequently, cells were harvested by centrifugation (1000 rpm or 300 g for 4 min) and re-suspended in mTeSR1 containing ROCKi. 120,000 cells were then seeded into each LN521-coated well and incubated for 30 min at 37°C. To remove non-specifically bound cells in the uncoated region, cells were washed once with PBS--, then switched to mTeSR1 and incubated for 1 h at 37°C (no ROCKi contained). Treatment cocktails described in the text were then added. Neural induction was performed in N2B27 medium supplemented with SB431542 (10 µM; Fisher Scientific) and LDN193189 (100 nM; Fisher Scientific). N2B27 was prepared by filtering a mixture of 24 mL DMEM/F12 (Corning), 24 mL Neurobasal media (Life Technologies), 0.5 mL N2 supplement (Fisher Scientific), 1 mL B27 supplement without vitamin A (Fisher Scientific), 0.5 mL Glutamax (Gibco) and 50 µL $beta$-mercaptoethanol (Gibco). In all experiments, the medium was replenished daily. However, when Wnt was added at D1.5, the medium was first replenished at D1.5 and then again at D3.

Immunostaining

Cells were fixed in 4% paraformaldehyde (Electron Microscopy Science) for 10 min at room temperature, followed by one PBS-- wash. Fixed samples were then permeabilized for 30 min at room temperature with blocking buffer (PBS-- with 0.1% Triton X-100 (Sigma-Aldrich) and 3% donkey serum (Sigma-Aldrich)). Primary antibodies were diluted in blocking buffer as listed in Table S1 and applied to samples overnight at 4°C (this is recommended for better staining rather than 2 h at room temperature). Samples were then sequentially washed three times with PBST (PBS with 0.1% Tween 20 (Sigma-Aldrich), 10 min each time), incubated for 30 min at room temperature with secondary antibodies (Table S1) supplemented with DAPI (1:1000), and washed three times with PBST in the same manner as before. For chips, coverslips were then mounted in Fluoromount-G (Southern Biotech) and allowed to dry in the dark for several hours. For the 96-well plate, samples were kept in PBS-- and were ready for imaging.

Single-molecule fluorescence in situ hybridization

Cells were fixed in 4% paraformaldehyde for 10 min at room temperature. smFISH was performed following the manufacturer's instructions (ACD Bio, RNAscope Multiplex Fluorescent v2 Assay). Probes are listed in Table S1.

Imaging

Fixed cell imaging

All images were acquired at 10× (NA 0.40, zoom 1.7x) and 30× (NA 1.05, zoom 2x) using an Olympus FV1200 laser scanning confocal microscope (LSM) with FV10-ASW 4.2 software.

Live cell imaging

TCF/LEF1:H2B-GFP H9 cells were seeded in multiple wells of a 96-well plate and differentiated as described above. Five colonies (700 μm) per well were imaged using a 20× (NA 0.75) objective on Olympus/Andor spinning disk confocal microscope. Every 1 h, multiple z-planes were acquired per position and three positions were set to cover one colony. Imaging was halted for a short period to replenish media at the exact replenishing time in the fixed cell experiment. Cells were maintained in a chamber at 37°C and 5% CO_2 throughout the duration of imaging.

Image analysis

All experiments were repeated at least twice with consistent results. 'n' in the figure captions denotes the number of micropatterns imaged per condition in the same experiment. Colonies were selected solely based on images from brightfield or DAPI channel without considering other channels to avoid observer bias.

Images were batch-stitched using FIJI with a Python script (Schindelin et al., 2012). Other analyses were performed using customized MATLAB code, available at `https://github.com/warmflashlab/Du2025Novel`. Micropatterned colonies were automatically identified, and then the edge or the center of the colony was defined, and a specified marker was quantified as a function of intensity versus distance to the edge/center. Distance was binned in 5 μm increments, estimated to be the radius of a cell. The mean intensity was averaged over all the colonies in that condition and error bars represent the standard error of the mean intensity.

Single-cell RNA sequencing analysis

The mouse single-cell RNA-sequencing dataset was acquired from Pijuan-Sala et al., 2019 and was normalized using Scanpy and scVI-tools (Gayoso et al., 2022; Wolf et al., 2018). A UMAP plot of all cell fates was generated to compare with the original plot and verify the reproducibility of our normalization. Only cell fates relevant to our study were selected: rostral neuroectoderm, caudal neuroectoderm, forebrain/midbrain/hindbrain, spinal cord, neuromesodermal progenitor (NMP). These cell types and stages were plotted again in UMAP to assist in the interpretation of the spatial and temporal expression of the genes of interest. The normalized data and code are available at `https://github.com/warmflashlab/Du2025Novel`.

Acknowledgments

We would like to thank Zachary Kingston for programming advice and Uny Tian for assistance with FISH staining. This work was funded by National Institutes of Health awards R01GM126122 and R35GM149328.

References

Andre, P., H. Song, W. Kim, A. Kispert, and Y. Yang (2015). "Wnt5a and Wnt11 regulate mammalian anterior-posterior axis elongation". In: *Development* 142.8, pp. 1516–1527.

Bouwmeester, T., S.-H. Kim, Y. Sasai, B. Lu, and E. M. D. Robertis (1996). "Cerberus is a head-inducing secreted factor expressed in the anterior endoderm of Spemann's organizer". In: *Nature* 382.6592, pp. 595–601.

Britton, G., I. Heemskerk, R. Hodge, A. A. Qutub, and A. Warmflash (2019). "A novel self-organizing embryonic stem cell system reveals signaling logic underlying the patterning of human ectoderm". In: *Development* 146.20, dev179093.

Broccoli, V., E. Boncinelli, and W. Wurst (1999). "The caudal limit of Otx2 expression positions the isthmic organizer". In: *Nature* 401.6749, pp. 164–168.

Camus, A., A. Perea-Gomez, A. Moreau, and J. Collignon (2006). “Absence of Nodal signaling promotes precocious neural differentiation in the mouse embryo”. In: *Developmental biology* 295.2, pp. 743–755.

Canning, C. A., L. Lee, C. Irving, I. Mason, and C. M. Jones (2007). “Sustained interactive Wnt and FGF signaling is required to maintain isthmic identity”. In: *Developmental biology* 305.1, pp. 276–286.

Chambers, S. M., C. A. Fasano, E. P. Papapetrou, M. Tomishima, M. Sadelain, and L. Studer (2009). “Highly efficient neural conversion of human ES and iPS cells by dual inhibition of SMAD signaling”. In: *Nature biotechnology* 27.3, pp. 275–280.

Chen, B., H. Khan, Z. Yu, L. Yao, E. Freeburne, K. Jo, C. Johnson, and I. Heemskerk (2025). “Extended culture of 2D gastruloids to model human mesoderm development”. In: *Nature Methods*, pp. 1–11.

Chhabra, S., L. Liu, R. Goh, X. Kong, and A. Warmflash (2019). “Dissecting the dynamics of signaling events in the BMP, WNT, and NODAL cascade during self-organized fate patterning in human gastruloids”. In: *PLoS biology* 17.10, e3000498.

Christian, J. L., B. J. Gavin, A. P. McMahon, and R. T. Moon (1991). “Isolation of cDNAs partially encoding four Xenopus Wnt-1int-1-related proteins and characterization of their transient expression during embryonic development”. In: *Developmental biology* 143.2, pp. 230–234.

Deglincerti, A., F. Etoc, M. C. Guerra, I. Martyn, J. Metzger, A. Ruzo, M. Simunovic, A. Yoney, A. H. Brivanlou, E. Siggia, et al. (2016). “Self-organization of human embryonic stem cells on micropatterns”. In: *Nature Protocols* 11.11, pp. 2223–2232.

Emiliani, V., E. Entcheva, R. Hedrich, P. Hegemann, K. R. Konrad, C. Lüscher, M. Mahn, Z.-H. Pan, R. R. Sims, J. Vierock, et al. (2022). “Optogenetics for light control of biological systems”. In: *Nature Reviews Methods Primers* 2.1, p. 55.

Fainsod, A., K. Deißler, R. Yelin, K. Marom, M. Epstein, G. Pillemer, H. Steinbeisser, and M. Blum (1997). “The dorsalizing and neural inducing gene follistatin is an antagonist of BMP-4”. In: *Mechanisms of development* 63.1, pp. 39–50.

Fu, J., A. Warmflash, and M. P. Lutolf (2021). “Stem-cell-based embryo models for fundamental research and translation”. In: *Nature materials* 20.2, pp. 132–144.

Gayoso, A., R. Lopez, G. Xing, P. Boyeau, V. Valiollah Pour Amiri, J. Hong, K. Wu, M. Jayasuriya, E. Mehlman, M. Langevin, Y. Liu, J. Samaran, G. Misrachi, A. Nazaret, O. Clivio, C. Xu, T. Ashuach, M. Gabitto, M. Lotfollahi, V. Svensson, E. da Veiga Beltrame, V. Kleshchevnikov, C. Talavera-López, L. Pachter, F. J. Theis, A. Streets, M. I. Jordan, J. Regier, and N. Yosef (Feb. 2022). “A Python library for probabilistic analysis of single-cell omics data”. In: *Nature Biotechnology*.

Glinka, A., W. Wu, H. Delius, A. P. Monaghan, C. Blumenstock, and C. Niehrs (1998). “Dickkopf-1 is a member of a new family of secreted proteins and functions in head induction”. In: *Nature* 391.6665, pp. 357–362.

Gouti, M., J. Delile, D. Stamataki, F. J. Wymeersch, Y. Huang, J. Kleinjung, V. Wilson, and J. Briscoe (2017). “A gene regulatory network balances neural and mesoderm specification during vertebrate trunk development”. In: *Developmental cell* 41.3, pp. 243–261.

Gouti, M., A. Tsakiridis, F. J. Wymeersch, Y. Huang, J. Kleinjung, V. Wilson, and J. Briscoe (2014). “In vitro generation of neuromesodermal progenitors reveals distinct roles for wnt signalling in the specification of spinal cord and paraxial mesoderm identity”. In: *PLoS biology* 12.8, e1001937.

Di-Gregorio, A., M. Sancho, D. W. Stuckey, L. A. Crompton, J. Godwin, Y. Mishina, and T. A. Rodriguez (2007). “BMP signalling inhibits premature neural differentiation in the mouse embryo”. In.

Hamburger, V. (1989). “The heritage of experimental embryology: Hans Spemann and the organizer”. In: *Journal of the History of Biology* 22.1.

Hammerschmidt, M., F. Pelegri, M. C. Mullins, D. A. Kane, F. J. v. Eeden, M. Granato, M. Brand, M. Furutani-Seiki, P. Haffter, C.-P. Heisenberg, et al. (1996). “Dino and mercedes, two genes regulating dorsal development in the zebrafish embryo”. In: *Development* 123.1, pp. 95–102.

Haremaki, T., J. J. Metzger, T. Rito, M. Z. Ozair, F. Etoc, and A. H. Brivanlou (2019). “Self-organizing neuruloids model developmental aspects of Huntington’s disease in the ectodermal compartment”. In: *Nature biotechnology* 37.10, pp. 1198–1208.

Heemskerk, I., K. Burt, M. Miller, S. Chhabra, M. C. Guerra, L. Liu, and A. Warmflash (2019). “Rapid changes in morphogen concentration control self-organized patterning in human embryonic stem cells”. In: *Elife* 8, e40526.

Hong, C.-S., B.-Y. Park, and J.-P. Saint-Jeannet (2008). “Fgf8a induces neural crest indirectly through the activation of Wnt8 in the paraxial mesoderm”. In.

Jo, K., S. Teague, B. Chen, H. A. Khan, E. Freeburne, H. Li, B. Li, R. Ran, J. R. Spence, and I. Heemskerk (2022). "Efficient differentiation of human primordial germ cells through geometric control reveals a key role for Nodal signaling". In: *Elife* 11, e72811.

Karzbrun, E., A. H. Khankhel, H. C. Megale, S. M. Glasauer, Y. Wyle, G. Britton, A. Warmflash, K. S. Kosik, E. D. Siggia, B. I. Shraiman, et al. (2021). "Human neural tube morphogenesis in vitro by geometric constraints". In: *Nature* 599.7884, pp. 268–272.

Kelly, G. M., P. Greenstein, D. F. Erezyilmaz, and R. T. Moon (1995). "Zebrafish wnt8 and wnt8b share a common activity but are involved in distinct developmental pathways". In: *Development* 121.6, pp. 1787–1799.

Kessel, M. and P. Gruss (1991). "Homeotic transformations of murine vertebrae and concomitant alteration of Hox codes induced by retinoic acid". In: *Cell* 67.1, pp. 89–104.

Kiecker, C. and C. Niehrs (2001). "A morphogen gradient of Wnt/β-catenin signalling regulates anteroposterior neural patterning in Xenopus". In: *Development*.

Kimura-Yoshida, C., H. Nakano, D. Okamura, K. Nakao, S. Yonemura, J. A. Belo, S. Aizawa, Y. Matsui, and I. Matsuo (2005). "Canonical Wnt signaling and its antagonist regulate anterior-posterior axis polarization by guiding cell migration in mouse visceral endoderm". In: *Developmental cell* 9.5, pp. 639–650.

Krauss, S., V. Korzh, A. Fjose, and T. Johansen (1992). "Expression of four zebrafish wnt-related genes during embryogenesis". In: *Development* 116.1, pp. 249–259.

Kumar, V., R. S. Goutam, S. Park, U. Lee, and J. Kim (2021). "Functional roles of FGF signaling in early development of vertebrate embryos". In: *Cells* 10.8, p. 2148.

Leyns, L., T. Bouwmeester, S.-H. Kim, S. Piccolo, and E. M. De Robertis (1997). "Frzb-1 is a secreted antagonist of Wnt signaling expressed in the Spemann organizer". In: *Cell* 88.6, pp. 747–756.

Lippmann, E. S., C. E. Williams, D. A. Ruhl, M. C. Estevez-Silva, E. R. Chapman, J. J. Coon, and R. S. Ashton (2015). "Deterministic HOX patterning in human pluripotent stem cell-derived neuroectoderm". In: *Stem cell reports* 4.4, pp. 632–644.

Liu, L., A. Nemashkalo, L. Rezende, J. Y. Jung, S. Chhabra, M. C. Guerra, I. Heemskerk, and A. Warmflash (2022). "Nodal is a short-range morphogen with activity that spreads through a relay mechanism in human gastruloids". In: *Nature communications* 13.1, p. 497.

Liu, P., M. Wakamiya, M. J. Shea, U. Albrecht, R. R. Behringer, and A. Bradley (1999). "Requirement for Wnt3 in vertebrate axis formation". In: *Nature genetics* 22.4, pp. 361–365.

Maden, M. (2002). "Retinoid signalling in the development of the central nervous system". In: *Nature Reviews Neuroscience* 3.11, pp. 843–853.

Martyn, I., A. H. Brivanlou, and E. D. Siggia (2019). "A wave of WNT signaling balanced by secreted inhibitors controls primitive streak formation in micropattern colonies of human embryonic stem cells". In: *Development* 146.6, dev172791.

Metzis, V., S. Steinhauser, E. Pakanavicius, M. Gouti, D. Stamataki, K. Ivanovitch, T. Watson, T. Rayon, S. N. M. Gharavy, R. Lovell-Badge, et al. (2018). "Nervous system regionalization entails axial allocation before neural differentiation". In: *Cell* 175.4, pp. 1105–1118.

Minn, K. T., Y. C. Fu, S. He, S. Dietmann, S. C. George, M. A. Anastasio, S. A. Morris, and L. Solnica-Krezel (2020). "High-resolution transcriptional and morphogenetic profiling of cells from micropatterned human ESC gastruloid cultures". In: *Elife* 9, e59445.

Moon, R. T., R. M. Campbell, J. L. Christian, L. L. McGrew, J. Shih, and S. Fraser (1993). "Xwnt-5A: a maternal Wnt that affects morphogenetic movements after overexpression in embryos of Xenopus laevis". In: *Development* 119.1, pp. 97–111.

Nieuwkoop, P. D. (1952). "Activation and organization of the central nervous system in amphibians. Part I. Induction and activation". In: *Journal of Experimental Zoology* 120.1, pp. 1–31.

Nieuwkoop, P. D. and G. Nigtevecht (1954). "Neural activation and transformation in explants of competent ectoderm under the influence of fragments of anterior notochord in urodeles". In: *Development* 2.3, pp. 175–193.

Ortiz-Salazar, M. A., E. Camacho-Aguilar, and A. Warmflash (2024). "Endogenous Nodal switches Wnt interpretation from posteriorization to germ layer differentiation in geometrically constrained human pluripotent cells". In: *bioRxiv*.

Pannese, M., C. Polo, M. Andreazzoli, R. Vignali, B. Kablar, G. Barsacchi, and E. Boncinelli (1995). "The Xenopus homologue of Otx2 is a maternal homeobox gene that demarcates and specifies anterior body regions". In: *Development* 121.3, pp. 707–720.

Petersen, C. P. and P. W. Reddien (2009). “Wnt signaling and the polarity of the primary body axis”. In: *Cell* 139.6, pp. 1056–1068.

Pijuan-Sala, B., J. A. Griffiths, C. Guibentif, T. W. Hiscock, W. Jawaid, F. J. Calero-Nieto, C. Mulas, X. Ibarra-Soria, R. C. Tyser, D. L. L. Ho, et al. (2019). “A single-cell molecular map of mouse gastrulation and early organogenesis”. In: *Nature* 566.7745, pp. 490–495.

Rhinn, M. and M. Brand (2001). “The midbrain–hindbrain boundary organizer”. In: *Current opinion in neurobiology* 11.1, pp. 34–42.

Rifes, P., M. Isaksson, G. S. Rathore, P. Aldrin-Kirk, O. K. Møller, G. Barzaghi, J. Lee, K. L. Egerod, D. M. Rausch, M. Parmar, et al. (2020). “Modeling neural tube development by differentiation of human embryonic stem cells in a microfluidic WNT gradient”. In: *Nature biotechnology* 38.11, pp. 1265–1273.

Rossant, J. and P. P. Tam (2021). “Opportunities and challenges with stem cell-based embryo models”. In: *Stem Cell Reports* 16.5, pp. 1031–1038.

Rowitch, D. H. and A. P. McMahon (1995). “Pax-2 expression in the murine neural plate precedes and encompasses the expression domains of Wnt-1 and En-1”. In: *Mechanisms of development* 52.1, pp. 3–8.

Sasai, Y., B. Lu, H. Steinbeisser, D. Geissert, L. K. Gont, and E. M. De Robertis (1994). “Xenopus chordin: a novel dorsalizing factor activated by organizer-specific homeobox genes”. In: *Cell* 79.5, pp. 779–790.

Schindelin, J., I. Arganda-Carreras, E. Frise, V. Kaynig, M. Longair, T. Pietzsch, S. Preibisch, C. Rueden, S. Saalfeld, B. Schmid, et al. (2012). “Fiji: an open-source platform for biological-image analysis”. In: *Nature methods* 9.7, pp. 676–682.

Schulte-Merker, S., K. J. Lee, A. P. McMahon, and M. Hammerschmidt (1997). “The zebrafish organizer requires chordino”. In: *Nature* 387.6636, pp. 862–863.

Shibata, M., M. Itoh, H. Hikasa, S. Taira, and M. Taira (2005). “Role of crescent in convergent extension movements by modulating Wnt signaling in early Xenopus embryogenesis”. In: *Mechanisms of development* 122.12, pp. 1322–1339.

Shimamura, K. and J. L. Rubenstein (1997). “Inductive interactions direct early regionalization of the mouse forebrain”. In: *Development* 124.14, pp. 2709–2718.

Simeone, A., D. Acampora, M. Gulisano, A. Stornaiuolo, and E. Boncinelli (1992). “Nested expression domains of four homeobox genes in developing rostral brain”. In: *Nature* 358.6388, pp. 687–690.

Simeone, A., D. Acampora, A. Mallamaci, A. Stornaiuolo, M. R. D’Apice, V. Nigro, and E. Boncinelli (1993). “A vertebrate gene related to orthodenticle contains a homeodomain of the bicoid class and demarcates anterior neuroectoderm in the gastrulating mouse embryo.” In: *The EMBO journal* 12.7, pp. 2735–2747.

Smith, W. C. and R. M. Harland (1992). “Expression cloning of noggin, a new dorsalizing factor localized to the Spemann organizer in Xenopus embryos”. In: *Cell* 70.5, pp. 829–840.

Spemann, H. and H. Mangold (1924). “über Induktion von Embryonalanlagen durch Implantation artfremder Organisatoren”. In: *Archiv für mikroskopische Anatomie und Entwicklungsmechanik* 100, pp. 599–638.

Stern, C. D. (2001). “Initial patterning of the central nervous system: how many organizers?” In: *Nature Reviews Neuroscience* 2.2, pp. 92–98.

— (2006). “Neural induction: 10 years on since the ‘default model’”. In: *Current opinion in cell biology* 18.6, pp. 692–697.

Tsakiridis, A., Y. Huang, G. Blin, S. Skylaki, F. Wymeersch, R. Osorno, C. Economou, E. Karagianni, S. Zhao, S. Lowell, et al. (2014). “Distinct Wnt-driven primitive streak-like populations reflect in vivo lineage precursors”. In: *Development* 141.6, pp. 1209–1221.

Tzouanacou, E., A. Wegener, F. J. Wymeersch, V. Wilson, and J.-F. Nicolas (2009). “Redefining the progression of lineage segregations during mammalian embryogenesis by clonal analysis”. In: *Developmental cell* 17.3, pp. 365–376.

Wang, S., M. Krinks, K. Lin, F. P. Luyten, and M. Moos (1997). “Frzb, a secreted protein expressed in the Spemann organizer, binds and inhibits Wnt-8”. In: *Cell* 88.6, pp. 757–766.

Warmflash, A., B. Sorre, F. Etoc, E. D. Siggia, and A. H. Brivanlou (2014). “A method to recapitulate early embryonic spatial patterning in human embryonic stem cells”. In: *Nature methods* 11.8, pp. 847–854.

Wolf, F. A., P. Angerer, and F. J. Theis (2018). “SCANPY: large-scale single-cell gene expression data analysis”. In: *Genome biology* 19, pp. 1–5.

Xue, X., Y. S. Kim, A.-I. Ponce-Arias, R. O’Laughlin, R. Z. Yan, N. Kobayashi, R. Y. Tshuva, Y.-H. Tsai, S. Sun, Y. Zheng, et al. (2024). “A patterned human neural tube model using microfluidic gradients”. In: *Nature* 628.8007, pp. 391–399.

Yamaguchi, T. P. (2001). “Heads or tails: Wnts and anterior–posterior patterning”. In: *Current Biology* 11.17, R713–R724.

Yamamoto, A., T. Nagano, S. Takehara, M. Hibi, and S. Aizawa (2005). “Shisa promotes head formation through the inhibition of receptor protein maturation for the caudalizing factors, Wnt and FGF”. In: *Cell* 120.2, pp. 223–235.

Zheng, Y., X. Xue, Y. Shao, S. Wang, S. N. Esfahani, Z. Li, J. M. Muncie, J. N. Lakins, V. M. Weaver, D. L. Gumucio, et al. (2019). “Controlled modelling of human epiblast and amnion development using stem cells”. In: *Nature* 573.7774, pp. 421–425.

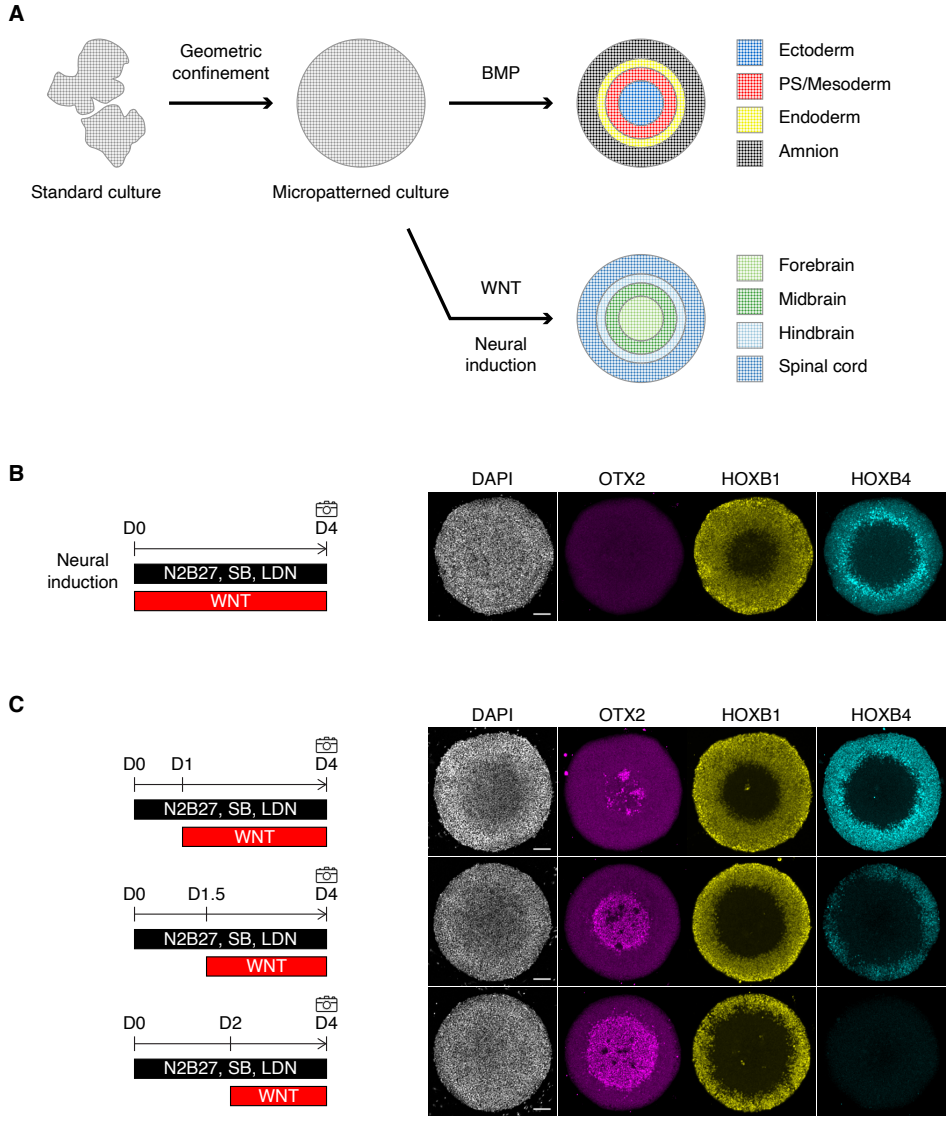

Figure 1: A novel self-organizing system to study anterior-posterior patterning. (A) Schematic comparing protocols for germ layer and neural AP axis micropatterns. (B, C) Representative immunofluorescence images of DAPI, OTX2, HOXB1, and HOXB4 following 4 days of neural induction combined with 300 $\mathrm{ng/mL}$ WNT3A treatment throughout (B) or with varying the time of addition as indicated (C). The colony diameter in B–C is 700 $\mu\mathrm{m}$. Scale bar, 100 $\mu\mathrm{m}$. Maximum intensity projection images are shown.

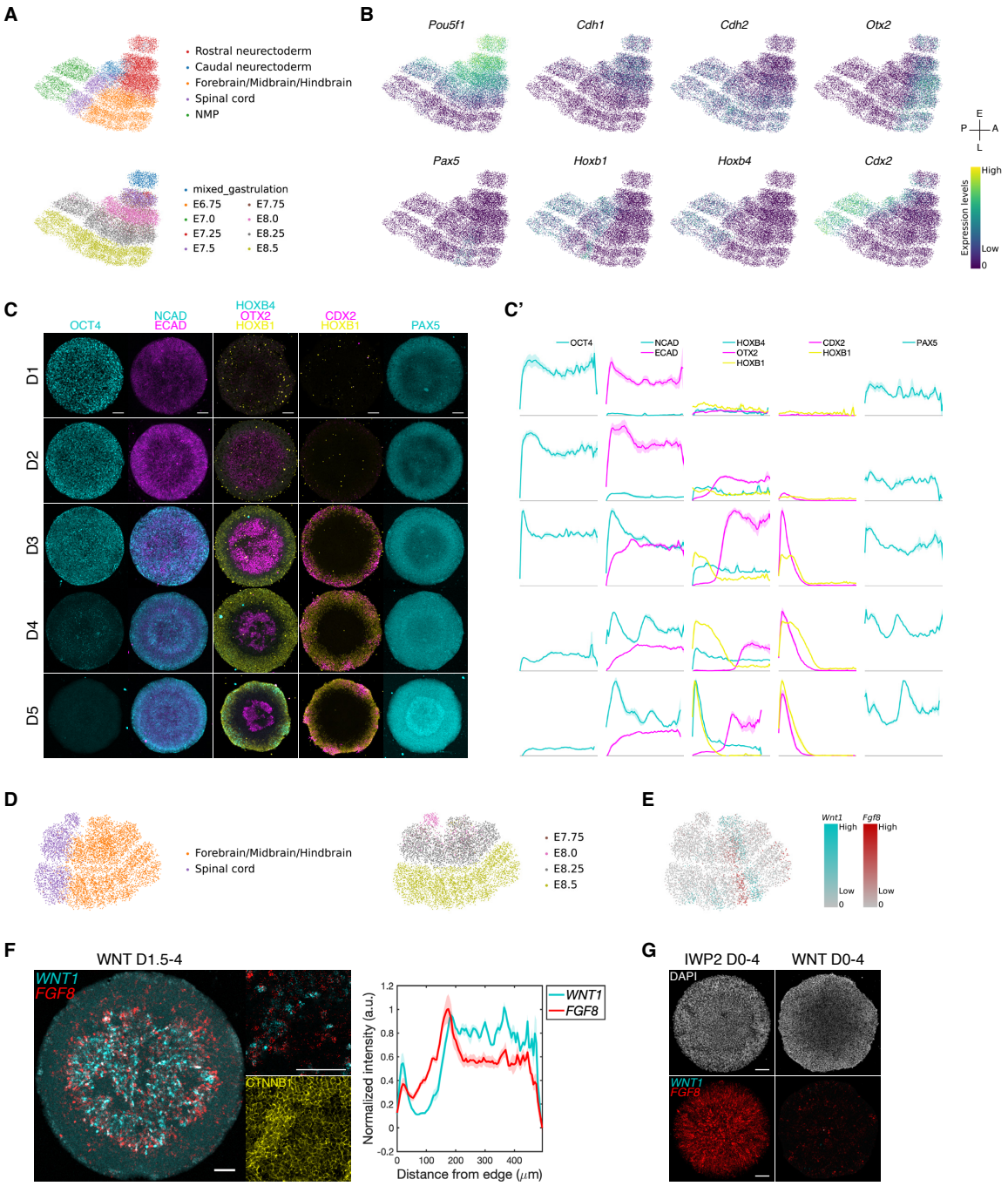

Figure 2: The micropatterned system recapitulates the dynamics of gene expression in mammalian embryos. (A) Uniform manifold approximation and projection (UMAP) plots display 14,937 selected cells from the mouse atlas dataset. Cells are colored by their cell-type (top) or developmental stage (bottom). (B) Expression levels of the indicated genes overlaid on the UMAP plot shown in A. (C) Representative immunofluorescence images of the indicated markers from D1–D5. WNT3A was added at D1.5 during the 5-day neural induction. (C') Quantification of the expression levels of the indicated markers as a function of distance from the colony edge on each day from D1–D5. (D) UMAP plots display 6610 selected cells from the mouse atlas dataset. Cells are colored by their cell-type (left) or developmental stage (right). (E) Expression levels of *Wnt1* (cyan) and *Fgf8* (red) overlaid on the UMAP plot shown in D. (F) Representative images of *WNT1* and *FGF8* mRNA expression, along with immunofluorescence for CTNNB1 ($beta$-catenin). The zoomed-in images represent a single z-plane. Quantification of the expression levels of *WNT1* and *FGF8*, normalized to DAPI intensity. (G) Representative images of *WNT1* and *FGF8* mRNA expression, along with DAPI staining. 4 μM IWP2 or 300 ng/mL WNT3A was added during the 4-day neural induction. The colony diameter in F is 1000 μm while in others it is 700 μm. Scale bar, 100 μm.

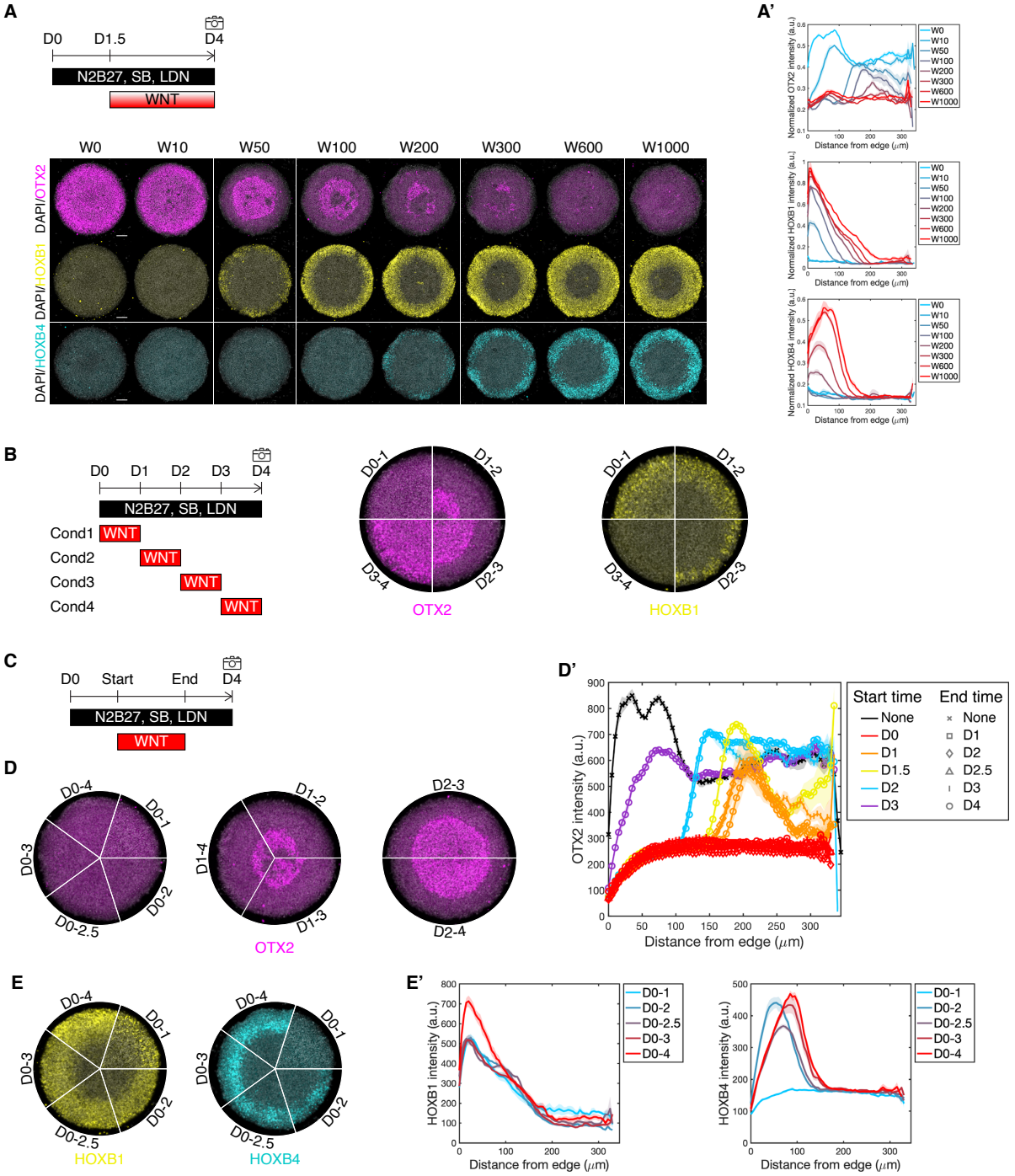

Figure 3: Timing is more critical than duration or concentration in cell fate decisions. (A) Representative immunofluorescence images of the indicated markers. The indicated concentrations of WNT3A (ng/mL) were added on D1.5. (A') Quantification of the expression levels of OTX2, HOXB1, and HOXB4 following the treatments described in A, normalized to DAPI intensity. (B) Representative immunofluorescence images of OTX2 and HOXB1. During the 4-day neural induction, WNT3A was added for 24 hours, at D0, D1, D2, or D3. (C) Schematic of the protocol shows cells treated with neural induction cocktail for 4 days, with varying start and end times of WNT3A, resulting in different durations. (D) Representative immunofluorescence images of OTX2, grouped by the start time of WNT3A treatment. (D') Quantification of the expression levels of OTX2. The lines are colored by the start time of Wnt treatment, and the marker shapes correspond to the end time. (E) Representative immunofluorescence images of HOXB1 and HOXB4, grouped by the start time of WNT3A treatment. (E') Quantification of the expression levels of HOXB1 and HOXB4.

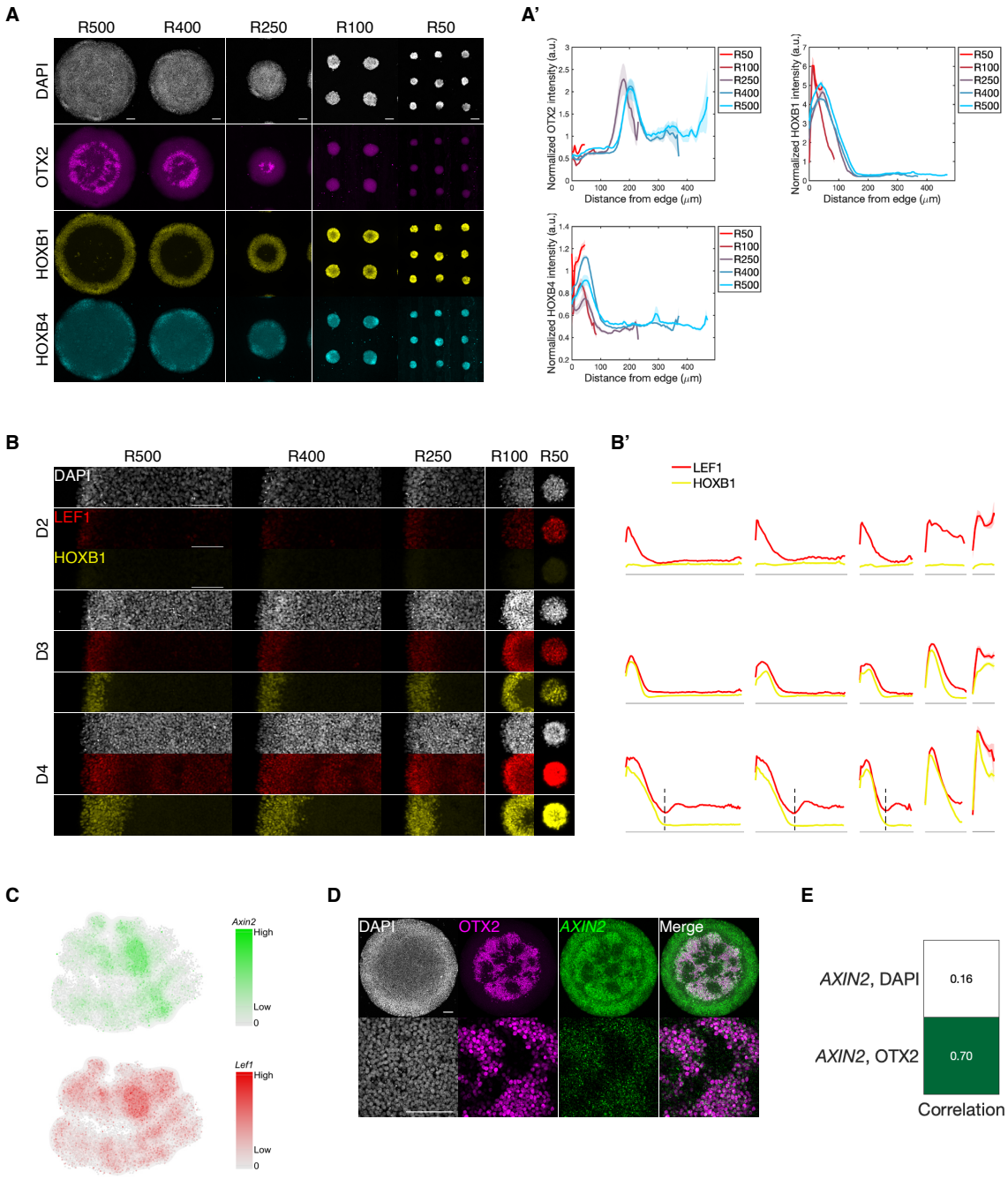

Figure 4: The midbrain-hindbrain border corresponds to a local minimum in Wnt signaling. (A) Representative immunofluorescence images of DAPI, OTX2, HOXB1 and HOXB4. The colonies vary in diameter, ranging from 500 μm to 50 μm. (A') Quantification of the expression levels of OTX2, HOXB1 and HOXB4, normalized to DAPI intensity. (B) Cropped representative immunofluorescence images of DAPI, LEF1 and HOXB1 at D2, D3 and D4. (B') Quantification of the expression levels of the indicated markers as a function of distance from the colony edge on each day from D2–D4. The dashed line indicates the corresponding HOXB1 levels at the point where Lef1 expression dips. (C) Kernel density estimate (KDE) plots show the estimated probability densities of *Axin2* and *Lef1* expression overlaid on the UMAP plot from Fig. 2D. (D) Representative images of *AXIN2* mRNA expression, along with DAPI and OTX2 staining. The bottom images show a zoomed-in view of the colony center. (E) Heatmap plot shows the Pearson correlation coefficient between *AXIN2* and DAPI, and between *AXIN2* and OTX2. As OTX2 protein and *AXIN2* mRNA are found in different cellular compartments, *AXIN2* images were Gaussian filtered with a sigma value of 16.7 pixels, which is approximately one-third of the major axis of the nucleus.

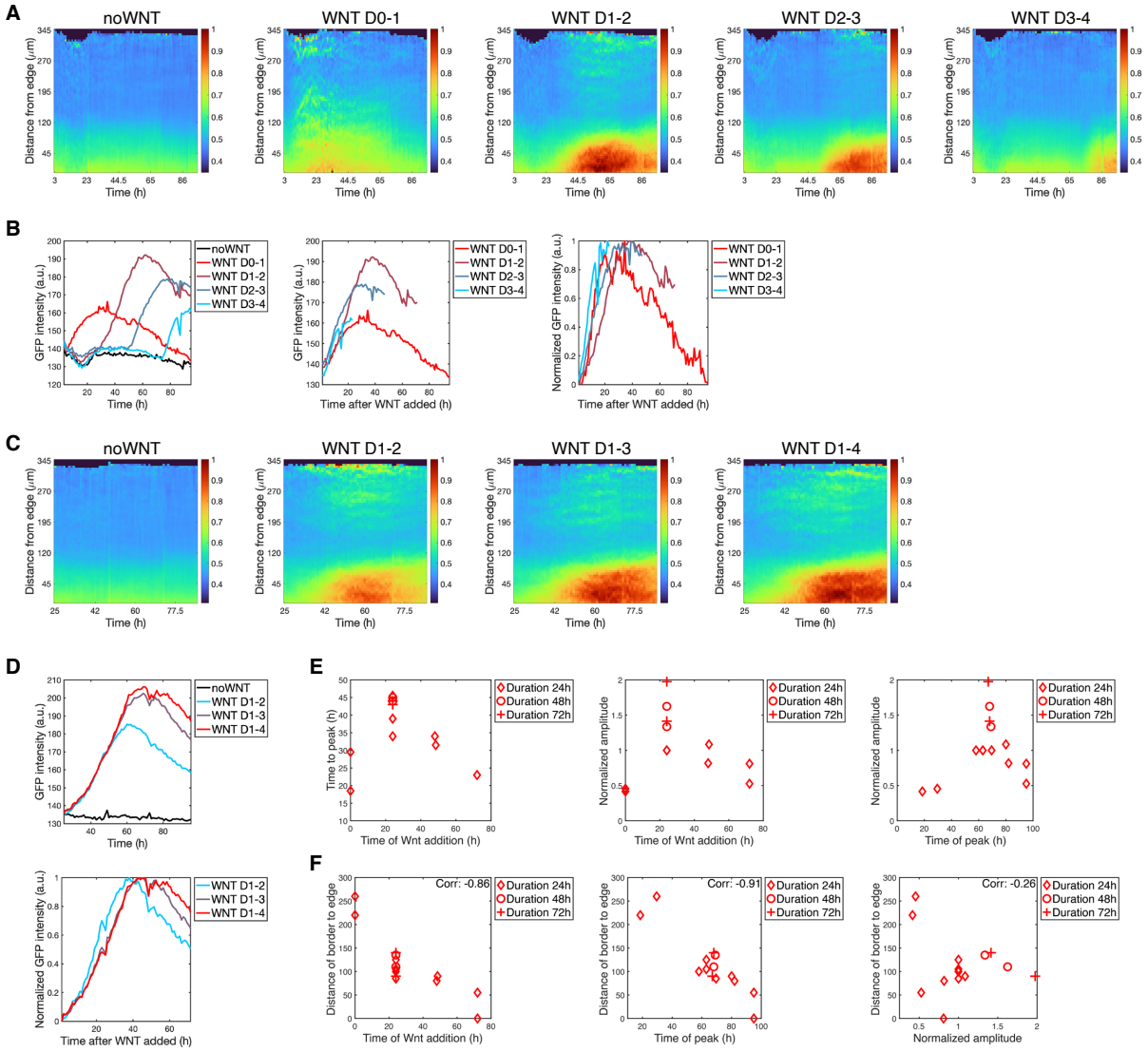

Figure 5: The timing of Wnt signaling determines the location of the border. (A, C) Heatmap plots of GFP levels, with the x-axis representing experimental time and the y-axis representing the distance from the colony edge, following 4 days of treatment with neural induction media and WNT3A as described in the labels. The colony diameter is 700 μm. (B, D) Quantification of average GFP intensity in the ring-shaped domain (0–100 μm from the edge). Normalized GFP intensity is calculated by scaling the GFP levels to their starting and maximum values. (E, F) The scatter plots combine experiments testing different Wnt durations and timings, with the marker shape indicating the duration. The time of Wnt addition, defined as the time when Wnt is added; the time of peak, defined as the time following the onset of differentiation when the Wnt reporter response reaches its maximum; the time to peak, defined as the time between the Wnt addition and the time of peak. Normalized amplitude refers to the amplitude of the Wnt response scaled by the conditions with no Wnt added, and WNT D1–2 as negative and positive conditions, respectively. (F) The distance from the border to the edge is quantified by summing the intensities of OTX2 and HOXB1, and measuring the distance from the edge to the dip in the summed intensity. The Pearson correlation coefficient between the two variables on the x- and y-axes is labeled in the top right corner.